EVALUATION OF TRANSFORM-BASED NUMERICAL METHODS APPLIED TO RICHARDS' EQUATION

Key Words: Richards' equation, transforms, finite elements, Newton-Galerkin, modified Picard

Robert G. Baca
Center for Nuclear Waste Regulatory Analyses
Southwest Research Institute, San Antonio, TX 78238-5166
Phone: (210) 522-3805 FAX: (210) 522-5155
internet: rbaca@swri.edu

Jacob N. Chung and David A. Stock
Washington State University, Pullman, WA

Revised
October 14, 1996

Submitted to *Advances in Water Resources*

EVALUATION OF TRANSFORM-BASED NUMERICAL METHODS APPLIED TO RICHARDS' EQUATION

Robert G. Baca
Center for Nuclear Waste Regulatory Analyses
Southwest Research Institute, San Antonio, TX

Jacob N. Chung and David A. Stock
Washington State University, Pullman, WA

ABSTRACT

Transform-based numerical approaches have been emerging as very promising computational approaches for solving the nonlinear infiltration model described by Richards' equation. These novel methods have been shown in the literature to yield improved robustness and computational speed over more conventional numerical algorithms. A computational study is presented that examines the relative advantages of three particular transforms: (i) natural log, (ii) inverse hyperbolic sine, and (iii) algebraic. These three transforms are implemented in numerical algorithms and evaluated using various test problems involving variably saturated flow in very dry and heterogeneous porous media. The performance of the numerical techniques is quantified in terms of computer execution time and global mass balance. The sensitivity of these two performance measures to boundary conditions, initial conditions, and soil heterogeneity is investigated. Numerical solutions obtained using the transform-based approaches in conjunction with a finite element technique are compared against the untransformed modified Picard and Newton-Galerkin finite element methods. The results of this comparative study show all three transform-based numerical algorithms and the untransformed Newton-Galerkin method are computationally faster than the untransformed modified Picard method. These transform-based methods achieve global mass balance equivalent to that of the modified Picard method. The algebraic transform algorithm was found to be superior with respect to accuracy. The overall finding of this study is that the Newton-Galerkin method, when applied directly to the mixed formulation of Richards' equation, is superior to all three transform-based numerical methods in both speed and robustness.

INTRODUCTION

Regulatory evaluations aimed at assessing the risks of waste disposal sites are making increasing use of detailed numerical models of flow and transport phenomena. Models of infiltration and deep percolation, in particular, are playing a central role in studies of waste disposal safety. In the case of low- and high-level nuclear waste disposal, for example, numerical models are currently being applied to forecast infiltration patterns that may occur as a result of climate changes (typically spanning thousands of years). In steady-state analyses, Monte Carlo simulations of flow are generally performed to develop probabilistic estimates of water fluxes[9] and travel times[5]. Such models require fast, accurate, and robust numerical algorithms for these specialized applications to become routine. This use of detailed simulation models has motivated research to pursue improved numerical techniques to solve the governing flow equation in a more efficient manner.

Although a variety of finite difference[8,15] and finite element techniques[16,17] are currently available for solving the nonlinear Richards' flow equation, these conventional techniques often work well for a limited class of flow conditions and simple hydrostratigraphic models. Moreover, existing techniques rarely exhibit the robustness and convergence rate desired for efficient three-dimensional, high-resolution simulations of flow in highly heterogeneous media.[1] Three particular types of simulation problems that pose the greatest computational difficulty are those involving (i) surface ponding on and high infiltration rates into very dry soils, (ii) flow involving the formation and dissipation of perched water zones, and (iii) flow through soil layers with large permeability contrasts. Test cases encompassing these types of hydraulic conditions and flow characteristics are considered in this paper.

Transform methods have historically been used in developing analytical solutions[20] to Richards' equation. Only recently, however, have researchers noted that numerical approximations to its various forms (i.e., mixed, head-based, and moisture-based) can be improved by introducing a special transform. For example, transform-based numerical approaches have been investigated by Baca et al.[2], Ross[26],

Kirkland et al.[21], and Pan and Wierenga.[23] Quite interestingly, the fact that these novel approaches can yield improved numerical performance has been, for the most part, empirically observed (i.e., a transform was tried and the numerical algorithm appeared to work better). Advocates of transform-based methods have not provided (i) rigorous mathematical arguments that explain "why" these novel approaches work better or (ii) quantified "how much" better (i.e., accuracy and robustness) they are than untransformed methods. Moreover, there has been a lack of in-depth numerical demonstrations that these transform-based approaches consistently yield more accurate and robust solutions for a wide range of flow problems of practical interest. Investigatiion of the latter aspect is the primary focus of this paper.

These distinct transform approaches can be unified through the use of a "partitioned transform" formulation which is presented herein. In this study, a general numerical solution algorithm is developed by discretizing the transformed governing equation using the Newton-Galerkin finite element method. The computational performance of these transform-based numerical algorithms is compared to that of the very competitive modified Picard finite element method[8] and the untransformed Newton-Galerkin method.

TRANSFORM-BASED APPROACHES

Transformed Flow Equation

The mixed form of Richards' equation for transient flow in variably-saturated porous media is a well-known nonlinear parabolic equation that is widely used in the hydrological sciences.[19] A modified form of this flow equation is obtained by making a simple change of variable in the spatial term. For one-dimensional (1D) flow and neglecting compressibility effects, the modified or "transformed" governing equation is expressed as

$$\frac{\partial \theta}{\partial t} = \frac{\partial}{\partial z}\left(\kappa(\psi)\frac{\partial \chi}{\partial z} - K(\psi)\right) \qquad (1)$$

where $\theta(\psi)$ is the volumetric water content (cm^3/cm^3), $\kappa(\psi)$ is $K\partial\psi/\partial\chi$, $K(\psi)$ is the hydraulic conductivity (cm/s), z is the depth (cm) taken positive downward, and ψ is the pressure head (cm). The

new dependent variable χ is defined as a generalized partitioned transform, namely

$$\chi = \left\{ \begin{array}{ll} \psi & \psi \geq \psi_0 \\ \alpha_1 f(\theta, \psi) + \alpha_2 & \psi < \psi_0 \end{array} \right\} \qquad (2)$$

where $f(\theta, \psi)$ is an analytic function yet to be specified and ψ_0 is an arbitrary match point. The fundamental idea of this approach is to select an analytic function that transforms ψ into a "compressed" state variable χ. This compression results in a smooth and more gradually varying solution space that in theory allows more accurate calculation of the spatial gradients of χ. In order for the partitioned transform to be appropriate, however, χ must be C^1 continuous at the match point ψ_0. Thus, the conditions constraining the choice of $f(\theta, \psi)$ are twofold

$$\psi_0 = \alpha_1 f(\theta_0, \psi_0) + \alpha_2 \qquad (3)$$

$$\frac{\partial \chi}{\partial \psi}\Big|_{\psi_0} = 1 = \alpha_1 \frac{\partial f(\theta_0, \psi_0)}{\partial \psi} \qquad (4)$$

where $\theta_0 = \theta(\psi_0)$. The previous two conditions are necessary for determining the two coefficients, α_1 and α_2. For the particular transforms considered, the match point pressure, ψ_0, was chosen to be zero. However, for transforms that depend on the soil hydraulic properties[15] the match point pressure is generally chosen close to the bubbling pressure.[3] Three transforms that can be written in a partitioned form and easily conform to Eqs. (3) and (4) are (i) natural log, (ii) inverse hyperbolic sine, and (iii) algebraic.

The natural log transform was originally developed and applied by Baca et al[2]. These authors implemented the log transform in the standard "head-based" formulation of Richards' equation, but in a manner limiting its application to purely unsaturated conditions. In the partitioned form described here, however, the log transform can be generalized to apply to both saturated and unsaturated regimes. It is expressed as

$$\chi_l = \left\{ \begin{array}{ll} \psi / S & \psi \geq 0 \\ \alpha_1 \log_e(-\psi / S + 1) + \alpha_2 & \psi < 0 \end{array} \right\} \tag{5}$$

where S is a normalizing constant. Applying Eqs. (3) and (4), it follows that

$$\frac{\partial \chi_l}{\partial \psi} = \left\{ \begin{array}{ll} 1 / S & \psi \geq 0 \\ 1 / (-\psi + S) & \psi < 0 \end{array} \right\} \tag{6}$$

where $\alpha_1 = -1$ and $\alpha_2 = 0$.

Building on the natural log transform idea, Ross[26] formulated the inverse hyperbolic sine transform, which he used in conjunction with the "mixed" formulation of Richards' equation given in Eq. (1). A simple modification of Ross' partitioned formulation is adopted here, namely

$$\chi_s = \left\{ \begin{array}{ll} \psi / S & \psi \geq 0 \\ \alpha_1 \log_e\left(\psi / S + \sqrt{1 + (\psi / S)^2}\right) + \alpha_2 & \psi < 0 \end{array} \right\} \tag{7}$$

which has the associated derivative relation

$$\frac{\partial \chi_s}{\partial \psi} = \left\{ \begin{array}{ll} 1 / S & \psi \geq 0 \\ 1 / \left(S\sqrt{1 + (\psi / S)^2}\right) & \psi < 0 \end{array} \right\} \tag{8}$$

where $\alpha_1 = 1$ and $\alpha_2 = 0$. Ross[26] noted that incorporation of the inverse hyperbolic sine in the mixed formulation yielded a numerical algorithm that better accommodated very dry initial conditions, but was less efficient than a method using the Kirchhoff transform.[27]

Recently, Pan and Wierenga[23] introduced a new transform which they incorporated into a semi-discrete form of Richards' equation, currently referred to in the technical literature as the "modified Picard" formulation.[8] This transform, which is designated here as the algebraic transform, is given by

$$\chi_a = \left\{ \begin{array}{ll} \psi & \psi \geq 0 \\ \alpha_1 \psi / (1 + S\psi) + \alpha_2 & \psi < 0 \end{array} \right\} \tag{9}$$

with the associated derivative

$$\frac{\partial \chi_a}{\partial \psi} = \left\{ \begin{array}{ll} 1 & \psi \geq 0 \\ 1/(1 + S\psi)^2 & \psi < 0 \end{array} \right\} \qquad (10)$$

where $\alpha_1 = 1$, $\alpha_2 = 0$, and S = empirical constant. It should be noted that this transform is slightly different than the others because S is an arbitrary parameter rather than a normalizing constant. Pan and Wierenga[23] presented results for a series of numerical test cases demonstrating the superiority of their transform over the standard modified Picard finite difference algorithm. In this comparative study, it was found that the algebraic transform performed best with $S = -0.001$ cm^{-1}.

Modified Picard Formulation

In a manner parallel to the aforementioned transform-based approaches, the so-called modified Picard method produces a "modified" form of Richards' equation. In this method, the governing equation is converted directly into a semi-discrete δ-based formulation, where δ is the incremental change in the pressure head and given by $\delta = \psi^{n+1,k+1} - \psi^{n+1,k}$. The indices n and k denote the time plane and iteration, respectively. This formulation, as described by Celia et al.[8], is obtained by expanding θ in the iteration space using a Taylor series. This semi-discrete formulation possesses two desirable properties (i) the algorithm exhibits excellent global mass balance, and (ii) the convergence rate is relatively insensitive to very dry soil conditions. This modified formulation is expressed as

$$C(\psi^k)\frac{\delta}{\Delta t} = \frac{\partial}{\partial z}\left[K(\psi^k)\left(\frac{\partial \delta}{\partial z} - 1\right)\right] + \frac{\partial}{\partial z}\left[K(\psi^k)\frac{\partial \psi^k}{\partial z}\right] - \frac{\Delta \theta^k}{\Delta t} \qquad (11)$$

where $\Delta\theta^k = \theta^{n+1,k} - \theta^n$.

This formulation, when further discretized using a finite element (or finite difference) method, does not, in the strictest sense, produce a Picard-type iteration algorithm because, in fact, it uses derivative information. This is fully transparent from the derivation of the above semi-discrete equation (see Appendix A). Thus, the numerical algorithm produced by the discretization of Eq. (11) is more

appropriately designated as "modified Newton" iteration. This characteristic explains, to a large degree, the superior convergence properties of this semi-discrete δ-based formulation over the classical Picard iteration method.[16,24]

FINITE ELEMENT ALGORITHM

Strategy for Transform-Based Numerical Solutions

Two general numerical strategies for solving the transformed Richards' equation have been presented in the literature. The first, and perhaps more common, strategy is to discretize the transformed equation and then linearize it using an iterative numerical algorithm in which the incremental change of the transform variable $\Delta\chi$ becomes the dependent variable. This "conventional transformation" has been used by Baca, et al.,[2] Hills, et al.,[15] Ross,[26] Kirkland, et al.,[21] and Pan and Wierenga.[23] Recently, Ross and Bristow[27] introduced an alternate strategy in which the transformed Richards' equation is discretized and then formulated in a iterative algorithm which is directly expressed in terms of the change in pressure head $\Delta\psi$. This "mixed transformation" was successfully applied by Baca et al.[3] using the transform developed by Hills et al.[15] and Kirkland et al.,[21]. The mixed transform strategy is more efficient for certain transforms primarily because it does not require computation of the inverse transform to evaluate $C(\psi)$ and $K(\psi)$. The conventional transformation, however, appears to permit the use of slightly larger starting time steps for some test cases but can encounter problems with floating point exceptions (i.e., overflow, invalid operand) during the calculation of the inverse transform. In this paper, we have elected to use the mixed transformation strategy for formulating the computational algorithms.

Newton-Galerkin Formulation

To formulate a numerical solution method for the transformed (or untransformed) Richards' equation, an iterative method[16,24] is typically used to accommodate its strong nonlinearity. An efficient iterative algorithm can be directly embedded in a finite element approximation by using the Newton-Galerkin method.[3] This method requires the product of a set of weighting functions, $\omega_j(z)$, and the first

order Taylor series expansion of the residual, ϵ^{k+1}, be orthogonal. Specifically, the Newton-Galerkin formulation requires

$$\int_{\Omega} \omega_j(z) \left(\epsilon^k + \frac{\partial \epsilon^k}{\partial \psi} \Delta \psi \right) dz = 0 \qquad 1 < j \leq N \tag{12}$$

where Ω denotes the spatial domain $0 \leq z \leq L$, N is the number of basis functions, and ϵ^k is obtained directly from the transformed Richards' equation, namely

$$\epsilon^k = \frac{\partial \theta}{\partial t} - \frac{\partial}{\partial z} \left(\kappa(\psi) \frac{\partial \chi}{\partial z} - K(\psi) \right) \tag{13}$$

In this expression, the spatial variation of θ, χ, κ, and K is approximated using the standard set of C^0 linear basis functions; these functions are chosen to be identical to the set of weighting functions $\omega_j(z)$. The transform variable χ, like ψ, is continuous at layer interfaces. In contrast, the quantities θ, κ, and K are discontinuous at soil layer interfaces because they depends on soil hydraulic properties. Substituting Eq. (13) into Eq. (12) and rearranging, the following system of algebraic equations is produced for an arbitrary element e

$$[J_e] \{\Delta \psi\} = -\{R_e\} \tag{14}$$

where the right handside vector is

$$\{R_e\} = \frac{1}{\Delta t} \int_{\Omega_e} \{\omega\} \{\omega\}^T dz \, \{\Delta \theta^k\} + \int_{\Omega_e} \left\{ \frac{\partial \omega}{\partial z} \right\} \kappa \left\{ \frac{\partial \omega}{\partial z} \right\}^T dz \, \{\chi\} - \int_{\Omega_e} \left\{ \frac{\partial \omega}{\partial z} \right\} \{\omega\}^T dz \, \{K\} - q^{bc} \begin{Bmatrix} \delta_{e1} \\ -\delta_{eM} \end{Bmatrix} \tag{15}$$

and the Jacobian matrix is given by

$$[J_e] = \frac{1}{\Delta t}\int_{\Omega_e}\{\omega\}\{\omega\}^T dz\,\{\Delta\theta^k\}\left\{\frac{\partial}{\partial\psi^{n+1}}\right\}^T \tag{16}$$

$$+\int_{\Omega_e}\left\{\frac{\partial\omega}{\partial z}\right\}\hat{\kappa}\left\{\frac{\partial\omega}{\partial z}\right\}^T dz\,\{\chi\}\left\{\frac{\partial}{\partial\psi^{n+1}}\right\}^T - \int_{\Omega_e}\left\{\frac{\partial\omega}{\partial z}\right\}\{\omega\}^T dz\,\{K\}\left\{\frac{\partial}{\partial\psi^{n+1}}\right\}^T$$

where $\hat{\kappa} = \{\omega\}^T\{\kappa\}$, the Kronecker deltas for the boundary flux q^{bc} are defined as $\delta_{e1} = 1$ for the first element and zero elsewhere, while $\delta_{eM} = 1$ for the last element only. Inserting the standard expressions for the 1D linear basis functions, $\{\omega\}^T = [1 - \xi / L_e\,,\ \xi / L_e]$, the individual terms of Eqs. (15) and (16) can be integrated exactly using the factorial formula[25]

$$\int_0^1 \xi_1^a \xi_2^b\, d1 = L_e \frac{a!\,b!}{(a+b+1)!} \tag{17}$$

where ξ is the local element coordinate, $(a\,,\,b)$ are integers, and L_e is the element length. Mass lumping[8] is applied to the time derivative terms in the previous equations to stabilize the matrices associated with the θ-terms. The fully integrated forms of $\{R_e\}$ and $[J_e]$ are

$$\{R_e\} = \frac{1}{\Delta t}\left(\frac{L_e}{2}\right)\{\Delta\theta^k\} - \overline{K}\begin{Bmatrix}-1\\1\end{Bmatrix} + \frac{1}{L_e}\,\overline{\kappa}\,\Delta\chi^k\begin{Bmatrix}-1\\1\end{Bmatrix} - \begin{Bmatrix}q_0^{bc}\\-q_L^{bc}\end{Bmatrix} \tag{18}$$

$$[J_e] = \frac{1}{\Delta t}\left(\frac{L_e}{2}\right)\begin{bmatrix}\partial\theta_1/\partial\psi_1 & 0\\ 0 & \partial\theta_2/\partial\psi_2\end{bmatrix} + \frac{1}{L_e}\,\overline{\kappa}\begin{bmatrix}\partial\chi_1/\partial\psi_1 & -\partial\chi_2/\partial\psi_2\\ -\partial\chi_1/\partial\psi_1 & \partial\chi_2/\partial\psi_2\end{bmatrix} \tag{19}$$

$$+\frac{\Delta\chi^k}{L_e}\begin{bmatrix}-\partial\overline{\kappa}/\partial\psi_1 & -\partial\overline{\kappa}/\partial\psi_2\\ \partial\overline{\kappa}/\partial\psi_1 & \partial\overline{\kappa}/\partial\psi_2\end{bmatrix} - \begin{bmatrix}-\partial\overline{K}/\partial\psi_1 & -\partial\overline{K}/\partial\psi_2\\ \partial\overline{K}/\partial\psi_1 & \partial\overline{K}/\partial\psi_2\end{bmatrix}$$

with $\Delta\chi^k = (\chi_2 - \chi_1)^{n+1,\,k}$. If prescribed, the flux terms q_0^{bc} and q_L^{bc} contribute to $\{R\}$ at the top and bottom boundaries. The quantities $\overline{\kappa}$ and $\overline{K}$ are computed as the arithmetic, geometric, or harmonic

mean values for the element. The elemental matrices for the untransformed Newton-Galerkin and modified Picard methods are presented in Appendix B.

Boundary Conditions

Incorporation of a fixed pressure head (Dirichlet condition) and/or specified flux (Neuman) boundary conditions are easily and naturally accommodated in the Newton-Galerkin finite element matrices. For example, in the case of a fixed pressure head, the entry for the global vector $\{R\}$ for node j is set to zero, and the corresponding diagonal term of $[J]$ set to 1 with the adjacent coefficients in the j-th row set to zero. The standard surface flux boundary condition and the free-drainage boundary at the base of the grid are directly incorporated into the right handside vector. For the special case of surface ponding, however, the surface flux boundary condition must be modified to include an additional storage term. In this study, the approach presented by Ross and Bristow[27] was used.

Iteration Strategy

After forming and solving the global forms of Eq. (14), the nodal values of the pressure head ψ are computed using the Newton iteration formula

$$\{\psi\}^{k+1} = \{\psi\}^{k} + \{\Delta\psi\}^{k} \qquad (20)$$

The quadratically convergent Newton algorithm can produce very large values of $\Delta\psi$ and, in turn, rapid changes in ψ. In certain cases, this can cause problems in evaluating $C(\psi)$ and $K(\psi)$. Thus, it is prudent to incorporate some form of damping[18,28] into the iteration algorithm. In this study, it was found that a simple and very effective method for achieving sufficient damping was to use the modified Newton (i.e., derivatives of $\overline{K}$ and $\overline{\kappa}$ in $[J]$ are neglected) for the first 2 iterations and the full Newton thereafter.

Convergence of the Newton iteration process was determined on the basis of the infinity norm of the residual error vector and the maximum relative change of the pressure head, ψ. Specifically, the

convergence was determined according to the criteria

$$\text{Max}\,|r_j^{(k+1)}| \le \epsilon_{res} \quad \text{and} \quad \text{Max}\,|\Delta\psi_j^{(k)} / \psi_j^{(k)}| \le \epsilon_{rel} \tag{21}$$

where $r_j^{(k+1)}$ is computed as $J\Delta\psi^{(k+1)} + R$. The convergence tolerances are generally chosen from the ranges: $10^{-9} \le \epsilon_{res} \le 10^{-5}$ (cm/s) and $10^{-8} \le \epsilon_{rel} \le 10^{-3}$ (unitless).

Grid Peclet and Courant Numbers

The nature and level of computational difficulties associated with the selected test problems were characterized in terms of the grid hydraulic Peclet number[10] Pe_{hg} and hydraulic Courant number Co_{hg}. As in computational fluid dynamics (CFD), the hydraulic Peclet number describes the relative significance of convective to diffusive transport. A Peclet number $Pe_{hg} > 1$ means that the convective (gravity) term in Richards' equation is more dominant than the diffusive (capillarity) term. The grid hydraulic Peclet number is calculated from

$$Pe_{hg} = -\frac{\partial}{\partial\psi}[\ln K(\psi)]\Delta z \tag{22}$$

where Δz is the element size. In high Peclet number flows, the hydraulic Courant number is a useful parameter for controlling the time stepping. A grid based hydraulic Courant number can be related to the Peclet number, namely $Co_{hg} = Pe_{hg}\Delta t\, K(\psi) / \Delta z$. The Courant number is used to calculate a characteristic time step $\Delta\tau_{hg}$ for a computational element. By analogy to its use in CFD[11], the Courant number provides a relationship for selecting the maximum step, namely

$$\Delta\tau_{hg} = \frac{Co_{hg}}{Pe_{hg}} \frac{\Delta z}{K(\psi)} \tag{23}$$

By fixing the maximum value of the Courant number, the above equation can be used to compute the maximum time step size.

Time-Stepping Strategy

Even though Eqs. (15) and (16) use a fully implicit time approximation, the time step size Δt must be constrained because it has a strong impact on the solution accuracy and number of Newton iterations. To advance the numerical solution through time in an efficient manner, an automatic time-stepping procedure was used. The procedure consisted of changing the time step in relation to: (i) the number of iterations required in the previous time plane and (ii) maximum incremental change (per time step) in water saturation level. Specifically, the time step was calculated according to the formula

$$\Delta t^{n+1} = \mathrm{Min}\left[f_1(k) , f_2(\delta S) \right] \Delta t^n \qquad (24)$$

where the scale factor $f_1(k)$ is a function of the total number of iterations (of the prior step) and is chosen so that a target number of iterations (e.g., $4 \le k \le 7$) is generally maintained, with the other scale factor given by

$$f_2(\delta S) = \delta S_e / \delta S_{\max} \qquad (25)$$

where δS_e is the desired change in saturation (typically 0.05 to 0.20) and $\delta S_{\max} = \mathrm{Max} \left| S_j^n - S_j^{n-1} \right|$. In addition, the time step calculated from Eq. (24) was constrained such that $\Delta t^n / 20 \le \Delta t^{n+1} \le 2 \Delta t^n$. For high Peclet number flows, the maximum time step was further constrained in accordance with the hydraulic Courant number (i.e., $\Delta t_{\max} \le \Delta \tau_{hg}$). The minimum time step size is specified by user input. In the test cases considered in this study, the minimum step size was typically set to 10^{-3} seconds.

If the iterative solution failed to converge within the specified maximum iterations (e.g., $k_{\max} = 12$), a smaller time step equal to half the previous value was automatically chosen and the solution repeated. This step reduction strategy was limited to a total of 15 consecutive halvings, at which point the solution was judged nonconvergent and the computer solution terminated.

VERIFICATION OF COMPUTER CODES

The previously described numerical algorithms were incorporated into a set of computer codes written in FORTRAN 77. The finite element codes used common routines to ensure consistency and permit direct intercomparisons. These codes were verified with a set of test problems taken from the technical literature[8,12,15,23,27]. Results from two verification test cases are presented in the following paragraphs. These two verification problems were selected because they represent contrasting boundary conditions and soil properties. All numerical simulations were performed using convergence tolerances of $\epsilon_{res} \leq 10^{-6}$ and $\epsilon_{rel} \leq 10^{-6}$. Code runs presented in this paper were performed on a Micron Millenia Pro 200 personal computer. The codes were compiled using the Lahey FORTRAN compiler and all calculations were performed in double precision.

Verification Example 1

The first example problem was adapted from Forsyth et al.,[12] and involves modeling infiltration into a deep caisson with relatively dry soil. The test problem is based on a field experiment conducted at the Los Alamos National Laboratory. The soil column is 600 cm and assumed to be a homogeneous Bandelier tuff. The soil hydraulic properties are described by the van Genuchten[30] formulas with parameters $\theta_r = 0.0$, $\theta_s = 0.33$, $K_s = 25.82$ cm/d, $\alpha = 0.0143$ 1/cm, and $n = 1.506$.

The initial pressure head profile was set to $\psi_i = -10^4$ cm. The upper boundary condition was a constant flux of $q_0^{bc} = 20.0$ cm/d at the soil surface, which is only slightly less than the hydraulic conductivity of the Bandelier tuff. The bottom boundary was held at the initial pressure head, ψ_i. A uniform mesh of 75 finite elements with $\Delta z = 8$ cm was used to represent the flow domain. A time period of 6 days was simulated using the previously described automatic time stepping algorithm.

The pressure head profiles computed with the five codes are presented in Fig. 1. This graphical comparison shows that the results of the transformed and untransformed algorithms agree with each other;

in addition, they exhibit very sharp fronts consistent with the published results of Forsyth et al.[12] It is noteworthy that the numerical solution produced by the algebraic transform exhibits a slightly sharper front. The CPU times for the five algorithms were: (i) Newton-Galerkin 14 s, (ii) natural log 15 s, (iii) inverse hyperbolic sine 15 s, (iv) algebraic 18 s, and (v) modified Picard 272 s.

Verification Example 2

The second example problem were taken from Pan and Wierenga[23] and consists of a homogeneous, moderately dry soil column with positive pressure head boundary conditions. The upper boundary condition is fixed at a constant pressure head consistent with ponded conditions. The combination of dry initial condition and ponded boundary conditions produce variably saturated flow from both boundaries to the center of the column. The soil hydraulic properties are described by the van Genuchten parameters θ_r = 0.1020, θ_s = 0.3658, K_s = 796.608 cm/d, α = 0.0335 1/cm, and n = 2.0.

The initial pressure head profile was set to $\psi_i = -10^3$ cm. The upper and lower boundary conditions were fixed at a positive pressure head value of ψ = 100 cm. The soil column was discretized into a uniform mesh of 50 finite elements with Δz = 2 cm. A time domain of 180 s was simulated using automatic time stepping.

The computed pressure head profiles are presented in Fig. 2. This comparison of numerical results shows the transformed and untransformed solutions agree very well. In addition, these results also replicate those in the paper by Pan and Wierenga.[23] As previously observed, the numerical solution produced by the algebraic transform is slightly sharper. The CPU times for the five algorithms were: (i) Newton-Galerkin 2 s, (ii) natural log 3 s, (iii) inverse hyperbolic sine 3 s, (iv) algebraic 3 s, and (v) modified Picard *incomplete* (execution was terminated because $\Delta t < 10^{-3}$ s were required for convergence).

Evaluation of Accuracy and Efficiency

Use of transform-based methods is predicated on the basic notion that the large gradients associated with ψ are much smaller in the transformed solution space for χ. This means that the "flux" term embedded in the discretized Richards' equation is more accurately calculated for the same Δz in the transformed case. This also suggests that larger grid spacing might be used without significant loss of accuracy. This characteristic was demonstrated by Ross and Bristow[27] using the Kirchhoff transform[16] which linearized the spatial term of Richards' equation.

The accuracy properties of the three transforms, as a function of discretization, were examined by considering the previous two verification examples. Numerical solutions were produced for progressively finer grids which were then compared to a "reference solution" obtained using an ultra-fine grid and smaller time steps. The accuracy of the successive numerical solutions was quantified in terms of the mean-square norm[6] of the error e defined by

$$\|e\|_0 = \left(\frac{1}{k} \sum_{i=1}^{k} e_i^2 \right)^{1/2} = \left[\frac{1}{k} \sum_{i=1}^{k} (\Psi_i - \psi_i)^2 \right]^{1/2} \qquad (26)$$

where Ψ_i is the reference pressure head at node i (calculated with the ultra-fine grid), ψ_i calculated pressure head at node i, and k is the number of comparison points. This norm measures the root mean square (RMS) discretization error which is bounded[6] by

$$\|e\|_0 \leq C \Delta z^p \qquad (27)$$

where C is a constant and p is an integer which is measure of the rate of convergence. The rate of convergence p for the transformed and untransformed solutions can be estimated by plotting the RMS on a log-log plot.

In the case of Verification Example 1, the RMS values were calculated for four uniform grids

consisting of 75, 150, 300, and 600 elements with the reference solution produced on a 1200 element grid. Similarly, for Verification Example 2, numerical solutions on grids composed of 50, 100, 200, and 500 elements were compared against a reference solution produced on a 1000 element grid. The RMS values obtained for three transforms and the Newton-Galerkin method are summarized graphically in Fig. 3.

The plot (see Fig. 3a) for the first verification example showed that the solutions produced with the algebraic transform were consistently more accurate than the other numerical methods. This was also true in the case of the second verification example (see Fig. 3b) but to a much lesser degree. It is important to note that RMS plots for the algebraic transform show a maximum slope $p \approx 3.24$ (i.e., cubic convergence) for the first verification example but $p \approx 1.08$ (i.e., superlinear convergence) for the second. In contrast, the maximum slopes for the other numerical methods are $p \leq 0.9$ for example 1 and $1.04 \leq p \leq 1.08$ for example 2. Quite interestingly, basic error theory for finite elements would suggest that the L^2 norm of error e should reduce quadratically with grid spacing (i.e., $\| e \|_0 \leq C_1 \Delta z^2$) for the case of finite elements with linear basis functions.[6]

To provide an indication of the computational efficiency of the various transformed-based methods and the Newton-Galerkin method, the Central Processor Unit (CPU) times for each run were plotted as a function of the number of elements. Calculational results for both verification examples are summarized in Figs. 4a and 4b. From these plots, it is evident the Newton-Galerkin method requires less CPU time with increasing grid refinement than the other transform-based methods. In contrast, the CPU time for the algebraic transform appears to increase much more rapidly with grid refinement.

DESCRIPTION OF FLOW SIMULATION PROBLEMS

To probe the computational capabilities (and vulnerabilities) of the various transform-based numerical algorithms, a set of diverse test problems was developed and solved. The aim of the test problems was to examine the performance of each algorithm as a function of surface fluid flux, initial

pressure head, and degree of perched water conditions. Initial and boundary conditions, as well as the spatial discretization, were chosen to make the test problems computationally difficult. These test conditions were woven into three hydrostratigraphic conceptual models chosen to approximate multilayer systems of actual sites located at (i) Yucca Mountain, Nevada; (ii) Idaho National Engineering Laboratory (INEL), Idaho; and (iii) Hanford Reservation, Washington.

Case 1 – Yucca Mountain Site

As part of an ongoing evaluation of Yucca Mountain for a proposed nuclear waste repository location, the U.S. Geological Survey has been studying the patterns of shallow infiltration in the Pagany Wash area of the Nevada Test Site. Boreholes in the alluvium channel of Pagany Wash were used to monitor the moisture content profiles and develop a 1D infiltration model.[13] A hydrostratigraphic model similar to that of Hevesi et al.,[14] was adopted for this test case. Soil hydraulic properties assigned to each layer are those reported for borehole UZN #7. Hevesi et al.,[14] used the soil property model of Brooks and Corey[7] to represent the hydraulic properties for the soil layers at this site. Parameters for this property model, taken from Hevesi et al.,[14] and the layer thicknesses are summarized in Table 1. The hydrostratigraphy was represented by a computational mesh of 135 elements of uniform size Δz = 10 cm. The average hydraulic conductivity $\overline{K}$ and transformed conductivity $\overline{\kappa}$ for each element were computed in the algorithm using the standard "arithmetic mean."

Case 2 – Idaho National Engineering Laboratory

In conjunction with environmental studies of the Radioactive Waste Management Complex (RWMC), researchers at INEL have modeled[4,22] subsurface flow from precipitation, snow melt, and drainage ditches to assess the potential for accelerating contaminant movement beneath the RWMC. The hydrostratigraphic setting of this site is characterized by layers of vesicular and massive basalt with a laterally continuous sedimentary interbed occurring at depth. Hydraulic properties for these layers are based on laboratory core measurements and curve fitting using van Genuchten parameters. The parameters

and thicknesses for each of these five layers are summarized in Table 2. A computational mesh of 300 elements was used to represent a 30-m region of the RWMC vadose zone; the element sizes were uniform with Δz = 10 cm. In this case, both the $\overline{K}$ and $\overline{\kappa}$ for each element were computed using the "harmonic mean" formula.

Case 3 – Hanford Reservation

A number of studies have been conducted to model the subsurface movement of a radioactive plume that occurred at the Hanford Reservation as a result of the T-106 tank leak. This tank leak occurred in the early 1970s at the 200 east area of the Hanford Reservation. Smoot and Sagar[29] modeled the migration of the liquid plume through the Hanford vadose zone to evaluate the likelihood of groundwater contamination. These authors modeled the stratified, glaciofluvial sediments at the site as a five-layer system spanning 63 m. Estimates of hydraulic properties for each layer were developed by Smoot and Sagar[29] using data from various locations at the Hanford Reservation. The parameters for the van Genuchten[30] soil property model are summarized in Table 3, which also gives layer thicknesses. For this test case, the domain was discretized into a computational mesh of 504 elements of uniform sizes, Δz = 12.5 cm. In this case, the $\overline{K}$ and $\overline{\kappa}$ for each element were computed using the "geometric mean" formula.

Definition of Case Studies

For each of the three sites previously described, a series of simulations was performed using various initial and boundary conditions specifically chosen to produce flow conditions with large pressure gradients, surface ponding, and/or formation and dissipation of perched water conditions. Four distinct combinations of initial and boundary conditions were considered for each site. The initial pressure heads were chosen to be representative of arid site conditions. The surface boundary conditions considered both fixed pressure head values and specified fluxes that are large relative to the permeability of selected soil layers. The bottom boundary condition was set to (i) a saturated condition to represent the presence of a

water table boundary or (ii) a free drainage condition. Specific conditions used in these cases are summarized in Table 4. In the first two INEL test cases, the initial pressure head at the surface node was set to 500 cm.

DISCUSSION OF SIMULATION RESULTS

The test cases adopted for the three arid sites (i.e., Yucca Mountain, INEL, and Hanford) were progressively more difficult and provided an effective means for probing the computational capabilities of both transform-based and untransformed numerical methods. As can be noted from Table 5, all five numerical methods successfully solved the test cases for Yucca Mountain; these test cases exhibited maximum $Pe_{hg} \approx 2$ but were not particularly difficult to solve. The INEL test cases exhibited similar grid Peclet numbers but were challenging because of the broad range of van Genuchten parameters. The Hanford test cases, with maximum $Pe_{hg} \approx 5$, posed the most computational difficulty and required large CPU times. The maximum Courant numbers used in these test cases to control time stepping are summarized in Table 6.

All the transform-based and untransformed numerical methods produced very small mass balance errors (see Table 7, errors reported without sign). The small mass balance errors observed in these calculations are because the five methods used the mixed formulation of Richards' equation which is inherently mass conservative. In performing simulations with the algebraic transform method, considerable experimentation was necessary to find the appropriate value for the empirical constant S. A value of $S = -0.001$ cm^{-1} (in contrast to the value of $S = -0.04$ cm^{-1} suggested by Pan and Wierenga[23]) yielded the best solutions for the set of test cases considered. It is uncertain, however, if the selected S value is optimal or universal.

As described in the following sections, all five numerical methods produced consistently accurate results for the Yucca Mountain site test cases. In contrast, the numerical algorithms generated distinct solutions for some of the INEL and Hanford test cases. These differences arose because of the coarseness

of the computational grid and the distinct accuracy properties of the numerical algorithms. Simulations with fine grids (generally consisting of twice as many finite elements) were performed to judge the accuracy of the individual numerical solutions; the fine grid results are presented in the sequence of graphical comparisons.

Comparison of Results for Yucca Mountain Test Cases

For the Yucca Mountain test cases, the numerical results of the four test runs (i.e., cases 1.1 through 1.4) indicated that all the transform-based and untransformed numerical methods were successful in handling the range of initial and boundary conditions and easily accommodated surface ponding and formation of perched water zones. The set of graphical comparisons in Figs. 5a and 5b clearly show excellent agreement among the various numerical results as well as with the fine grid solutions (shown as solid dots). Pressure head profiles for the algebraic transform suggest slightly better capability to capture steep fronts. As can be noted from Table 5, the three transforms exhibited comparable CPU times while the untransformed Newton-Galerkin method was consistently faster. The Newton-Galerkin method was 10 to 30 percent faster than the transform-based methods and more than 3 times faster than the popular modified Picard method.

Comparison of Results for INEL Test Cases

In the INEL test cases, the modified Picard and Newton-Galerkin methods solved all four cases (i.e., 2.1 through 2.4) but the accuracy achieved was limited by spatial discretization in two cases. The transform methods were generally slightly more accurate than the untransformed methods but only the algebraic transform algorithm successfully solved all four cases. The natural log and inverse hyperbolic sine transform methods were nonconvergent for the two cases with flux boundary conditions. The CPU times for the five numerical methods were quite varied; the Newton-Galerkin method generally exhibited the smallest execution times while the modified Picard and algebraic transform produced the largest (see Table 5).

Pressure head profiles for the first two cases are compared in Fig 6a. For case 2.1, it was observed that the five numerical methods produced a spread of numerical results. The Newton-Galerkin and modified Picard methods, for example, predicted the least penetration of the wetting front while the natural log and algebraic transform method yielded the deepest penetration. As can be seen from Fig. 6a, the fine grid (i.e., Δz = 5.0 cm) solution confirmed that the algebraic and natural log transform methods were the most accurate for this case. For case 2.2, the pressure head profiles produced by all methods except the algebraic transform showed a very close grouping (see Fig. 6a). The fine grid simulation, however, produced a profile with the front located at a depth of about 1000 cm and was more consistent with the group of solutions than with the algebraic transform result. The algebraic transform profile suggests a front at a depth of about 2000 cm which was an anomalous result. This suggested a degradation in the accuracy of the algebraic transform method which was inconsistent with the results of previous test case. Additional runs with smaller Courant numbers (to impose smaller time steps) were made with the algebraic transform code, however, no significant improvements in the simulation results were obtained. It was speculated that a different value of S may be required to achieve improved results with the algebraic transform.

Profiles calculated for the last two cases are compared in Fig 6b. For case 2.3, it was noted that the algebraic transform predicted a deeper penetration of the front than the profile generated with the fine grid. The modified Picard and Newton-Galerkin results were again indistinguishable while the natural log and inverse hyperbolic sine transforms solutions were nonconvergent. For case 2.4, the Newton-Galerkin and modified Picard profiles again overlaid perfectly, but underpredicted the location of the pressure front. Both the natural log and inverse hyperbolic sine transform methods were nonconvergent for this case, while the algebraic transform solution again yielded a deeper front location.

Comparison of Results for Hanford Reservation Test Cases

In the Hanford Reservation test cases, transform-based and untransformed algorithms produced numerical solutions for all four test runs (i.e., cases 3.1 through 3.4) that exhibited trends similar to those

of the previous of test cases. For instance, the algebraic transform was the most accurate while the modified Picard and Newton-Galerkin were the least accurate (relative to the fine grid results). The observed CPU times varied widely, however, the Newton-Galerkin method consistently produced the smallest execution times and the modified Picard yielded the largest (see Table 5).

Graphical comparisons of pressure head profiles for the first two test cases are presented in Fig. 7a. For case 3.1, the plot showed a spread of numerical solutions which, in fact, reflected the accuracy characteristics of each method. The modified Picard and Newton-Galerkin methods predicted a profile with a sharp front while the algebraic transform method profile indicated almost complete saturation of the soil column. The natural log and inverse hyperbolic transform methods predicted sharp pressure fronts but with deep penetration of the soil column. The fine grid (i.e., $\Delta z = 6.25$ cm) profile overlaid perfectly on the pressure head profile produced by the algebraic transform method. This result again demonstrated the higher accuracy of the algebraic transform method. For case 3.2, however, the algebraic transform method was nonconvergent while the other methods generated pressure head profiles that were virtually indistinguishable (see Fig 7a). The fine grid solution for this case, however, indicated a deeper penetration of the moisture front by about 1000 cm.

Comparisons for the other two test cases are presented in Fig. 7b. For case 3.3, the plot showed very close agreement among all methods. However, the fine grid solution for this case suggested that underpredicted the front location by about 1000 cm. For case 3.4, the natural log and inverse hyperbolic sine transform methods failed to produce convergent solutions. As in the previous case, the profile generated by the algebraic transform method indicated slightly greater penetration (than the modified Picard and Newton-Galerkin solutions). The fine grid results, however, suggest an under prediction of the front by about 900 cm.

SUMMARY AND CONCLUSIONS

A comparative study was performed to evaluate computational advantages of transform-based

numerical approaches for solving Richards' equation. These approaches used the natural log, inverse hyperbolic sine, and algebraic transforms to modify the governing equation. In turn, the transformed Richards' equation was discretized using a finite element method. These numerical methods were also compared against the untransformed modified Picard and Newton-Galerkin methods. To provide a broad basis of comparison, the transformed-based and untransformed finite element methods were applied to a total of 12 test cases. These test cases considered three layered vadose zones that are representative of actual arid sites. Various combinations of initial and boundary conditions were considered in flow simulations for each site. Performance of the computational methods was quantified in terms of CPU time and global mass balance error. The accuracy of the methods was qualitatively evaluated by comparisons with fine grid solutions generated with the Newton-Galerkin method.

Numerical results of this comparative study showed all three transform-based methods and the untransformed Newton-Galerkin method were computationally faster than the popular modified Picard method. In fact, these methods were typically two to five times faster than the modified Picard finite element method. For the range of test cases considered, the untransformed Newton-Galerkin method and modified Picard were found to be more robust than the transform-based methods but in a number of cases were less accurate. In certain test cases, the algebraic and natural log transform method were found to be substantially superior with respect to calculational accuracy on coarse grids. The accuracy properties of the algebraic transform, however, appeared to degrade significantly for cases with very dry initial pressure heads; it was conjectured that the high accuracy range of this transform may be dependent on value of the empirical constant S. The overall conclusion of this comparative study was that, while transform-based algorithms offer some accuracy benefits, they are not consistently superior to untransformed methods.

ACKNOWLEDGMENTS

The authors wish to thank Drs. S. Stothoff, G. Wittmeyer, and B. Sagar for their reviews and comments

on the original manuscript. The authors also thank Dr. J.D. Randall of the Nuclear Regulatory Commission (NRC) for his comments and suggestions. The research presented in this paper was funded by the NRC under Contract No. NRC-02-93-005 and was performed at the Center for Nuclear Waste Regulatory Analyses (CNWRA). The research was performed on behalf of the NRC Office of Nuclear Regulatory Research, Division of Regulatory Applications. The paper is an independent product of the CNWRA and does not necessarily reflect the views or regulatory position of the NRC. The FORTRAN codes used in the study are not under the CNWRA software configuration management procedure.

REFERENCES

1. Ababou, R., and L.W. Gelhar, A high-resolution finite difference simulator for 3D unsaturated flow in heterogeneous media, *Proceedings of Computational Methods in Water Resources*, Elsevier and Computational Mechanics Publications, London, UK, 1: 173–178, 1988.

2. Baca, R.G., I.P. King, and W.R. Norton, Finite element models for simultaneous heat and moisture transport in unsaturated soils, *Proceedings of the Second International Conference on Finite Elements in Water Resources*, Pentech Press, London, UK, 1.19–1.35, 1978.

3. Baca, R.G., J.N. Chung, and D.J. Mulla, Mixed transform finite element method for solving the equation for variably saturated flow in porous media, submitted to *Inter. J. Numer. Method in Fluids*, 1996.

4. Baca, R.G., S.O. Magnuson, H.D. Nguyen, and P. Martian, *A Modeling Study of Water Flow in the Vadose Zone Beneath the Radioactive Waste Management Complex*, EGG-GEO-10068, EG&G Idaho, Inc., Idaho Falls, ID, 1992.

5. Bagtzoglou, A.B., and R.G. Baca, Probabilistic calculations of groundwater travel time in heterogeneous three-dimensional porous media, *Mat. Res. Soc. Symp. Proc.*, 333: 849–854, 1994.

6. Becker, E.B., G.F. Carey, and J.T. Oden, *Finite Elements*, Vol. 1, Prentice Hall, Inc., Englewood Cliffs, NJ, 1981.

7. Brooks, R.H., and A.T. Corey, Properties of porous media affecting fluid flow, *J. Irrigation and Drainage Div., Proc. ASCE*, SER, IR2: 61–88, 1966.

8. Celia, M.A., E.T. Bouloutas, and R.L. Zarba, A general mass-conservative numerical solution for the unsaturated flow equation, *Water Resour. Res.*, 26(7): 1,483–1,496, 1990.

9. Childs, S.W., and A. Long, Model and calculations for net infiltration, *Proceeding of the Third Annual High-Level Radioactive Waste Management Conference*, American Nuclear Society, 2: 1,633–1,642, 1992.

10. Finlayson, B.A. *Nonlinear Analysis in Chemical Engineering*, McGraw-Hill International Book Company, New York, NY, 1980.

11. Fletcher, C.A.J. *Computational Techniques for Fluid Dynamics*, Vol 1 and 2, Springer-Verlag, New York, NY, 1988.

12. Forsyth, P.A., Y.S. Wu, and K. Pruess, Robust numerical methods for saturated-unsaturated flow with dry initial conditions in heterogeneous media, *Advances in Water Resources*, 18: 25-38, 1995.

13. Hevesi, J.A., and A.L. Flint, The influence of seasonal climatic variability on shallow infiltration at Yucca Mountain, *Proceedings of the Fourth Annual High-Level Radioactive Waste Management Conference*, American Nuclear Society, 1: 122–131, 1993.

14. Hevesi, J.A., A.L. Flint, and L.E. Flint, Verification of a one-dimensional model for predicting shallow infiltration at Yucca Mountain, *Proceedings of the Fifth Annual High-Level Radioactive Waste Management Conference*, American Nuclear Society, 2: 2,323–2,332, 1994.

15. Hills, R.G., I. Porro, D.B. Hudson, and P.J. Wierenga, Modeling one-dimensional infiltration into very dry soils, 1. Model development and evaluation, *Water Resour. Res.*, 25(6): 1,259–1,269, 1989.

16. Huyakorn, P.S., and G. Pinder, *Computational Methods in Subsurface Flow*, Academic Press, Inc., New York, NY, 1983.

17. Huyakorn, P.S., S.D. Thomas, and B.M. Thompson, Techniques for making finite elements competitive in modeling flow in variably saturated porous media, *Water Resour. Res.*, 20(8): 1,099–1,114, 1984.

18. Jennings, A. and J.J. McKneown, *Matrix Computation*, Second Edition, John Wiley & Sons, New York, NY, 1992.

19. Jury, W.A., W.R. Gardner, and W.H. Gardner, *Soil Physics*, Fifth Edition, John Wiley & Sons, New York, NY, 1993.

20. Kirkham, D. and W.L. Powers, *Advanced Soil Physics*, Wiley-Interscience, New York, NY, 1972.

21. Kirkland, M.R., R.G. Hills, and P.J. Wierenga, Algorithms for solving Richards' equation for variably saturated soils, *Water Resour. Res.*, 28(8): 2,049–2,058, 1992.

22. Martin, P., and C.S. Smith, *Benchmark and Partial Validation Testing of the FLASH Computer Code, Version 3.0*, EGG-ENV-10975, EG&G Idaho, Inc., Idaho Falls, ID, 1993.

23. Pan, L., and P.J. Wierenga, A transformed pressure head-based approach to solve Richards' equation for variably saturated soils, *Water Resour. Res.*, 31(4): 925–931, 1995.

24. Paniconi, C., and M. Putti, A comparison of Picard and Newton iteration in the numerical solution of multidimensional variably saturated flow problems, *Water Resour. Res.*, 30(12): 3,357–3,374, 1994.

25. Pepper, D.W., and J.C. Heinrich, *The Finite Element Method*, Taylor and Francis Publishing, Bristol, PA, 1992.

26. Ross, P.J., Efficient numerical methods for infiltration using Richards' equation, *Water Resour. Res.*, 26(4): 279–290, 1990.

27. Ross, P.J., and K.L. Bristow, Simulating water movement in layered and gradational soils using the Kirchhoff transform, *Soil Sci. Soc. Am. J.*, 54: 1,519–1,524, 1990.

28. Sewell, G., *Analysis of a Finite Element Method: PDE/PROTRAN*, Springer-Verlag, New York, NY, 1985.

29. Smoot, J.L., and B. Sagar, *Three-Dimensional Contaminant Plume Dynamics in the Vadose Zone: Simulation of the 241-T-106 Single Shell Tank Leak at Hanford*, PNL-7221, Pacific Northwest Laboratory, Richland, WA, 1990.

30. van Genuchten, M.T., A closed-form equation for predicting the hydraulic properties of unsaturated soils, *Soil Sci. Soc. Am. J.*, 44: 892–898, 1980.

APPENDIX A – DERIVATION OF MODIFIED PICARD METHOD

To derive the semi-discrete form of the modified Picard method, consider first the standard mixed formulation of Richards' equation, which is expressible in 1D form as

$$\frac{\partial \theta}{\partial t} = \frac{\partial}{\partial z}\left[K(\psi)\left(\frac{\partial \psi}{\partial z} - 1\right)\right] \tag{28}$$

First, discretize the accumulation term using a backward difference approximation. Thus,

$$\frac{\theta^{n+1} - \theta^{n}}{\Delta t} = \frac{\partial}{\partial z}\left[K(\psi)\left(\frac{\partial \psi}{\partial z} - 1\right)\right] \tag{29}$$

Because of the implicit nature of the backward difference approximation, it is understood that the spatial term on the right handside is at the $n+1$ time level. Next, use a Taylor series expansion in the "iteration space" to relate $\theta^{n+1,k+1}$ to $\theta^{n+1,k}$, namely

$$\theta^{n+1,k+1} = \theta^{n+1,k} + \frac{\partial \theta}{\partial \psi}\delta \tag{30}$$

with the incremental change in ψ being defined by

$$\delta = \psi^{n+1,k+1} - \psi^{n+1,k} \tag{31}$$

where k is the iteration index. Letting $C(\psi^k) = \partial\theta / \partial\psi$ and substituting Eq. (3) into (2), one obtains

$$\frac{\theta^{n+1,k} + C(\psi^k)\,\delta - \theta^{n}}{\Delta t} = \frac{\partial}{\partial z}\left[K(\psi)\left(\frac{\partial \psi}{\partial z} - 1\right)\right] \tag{32}$$

Next, let $\Delta\theta^k = \theta^{n+1,k} - \theta^n$ and rearrange Eq. (4) which yields

$$C(\psi^k)\frac{\delta}{\Delta t} = \frac{\partial}{\partial z}\left[K(\psi)\left(\frac{\partial \psi}{\partial z} - 1\right)\right] - \frac{\Delta\theta^k}{\Delta t} \tag{33}$$

The capillary diffusion term on the right handside can be written in terms of δ by adding and subtracting a similar diffusion expression but evaluated at the k-th iteration. Thus, one obtains the final form of the

semi-discrete "delta" formulation, referred to by Celia et al.,[7] as the modified Picard method,

$$C(\psi^k)\frac{\delta}{\Delta t} = \frac{\partial}{\partial z}\left[K(\psi^k)\left(\frac{\partial \delta}{\partial z} - 1\right)\right] + \frac{\partial}{\partial z}\left[K(\psi^k)\frac{\partial \psi^k}{\partial z}\right] - \frac{\Delta\theta^k}{\Delta t} \qquad (34)$$

This modified form of Richards' equation has one very important advantage (over the original equation) in that, when approximated using a finite element or finite volume method, it yields a computational algorithm which exhibits excellent global mass balance.

APPENDIX B – ELEMENTAL MATRICES

The elemental matrices for the untransformed Newton-Galerkin method can be obtained by simplifying Eqs. (18) and (19). The general expressions for the right handside vector and the Jacobian matrix are

$$\{R_e\} = \frac{1}{\Delta t}\left(\frac{L_e}{2}\right)\{\Delta\theta^k\} - \overline{K}\begin{Bmatrix}-1\\1\end{Bmatrix} + \frac{1}{L_e}\overline{K}\,\Delta\psi^k\begin{Bmatrix}-1\\1\end{Bmatrix} - \begin{Bmatrix}q_0^{bc}\\-q_L^{bc}\end{Bmatrix} \qquad (35)$$

$$[J_e] = \frac{1}{\Delta t}\left(\frac{L_e}{2}\right)\begin{bmatrix}\partial\theta_1/\partial\psi_1 & 0\\ 0 & \partial\theta_2/\partial\psi_2\end{bmatrix} + \frac{1}{L_e}\overline{K}\begin{bmatrix}1 & -1\\ -1 & 1\end{bmatrix} \qquad (36)$$
$$\left(\frac{\Delta\psi^k}{L_e} - 1\right)\begin{bmatrix}-\partial\overline{K}/\partial\psi_1 & -\partial\overline{K}/\partial\psi_2\\ \partial\overline{K}/\partial\psi_1 & \partial\overline{K}/\partial\psi_2\end{bmatrix}$$

The elemental matrices for the modified Picard method are derived using the standard Bubnov-Galerkin procedure and the integration formula given in Eq. (17). The resulting elemental matrices are

$$\{R_e\} = \frac{1}{\Delta t}\left(\frac{L_e}{2}\right)\{\Delta\theta^k\} - \overline{K}\begin{Bmatrix}-1\\1\end{Bmatrix} + \frac{1}{L_e}\overline{K}\,\Delta\psi^k\begin{Bmatrix}-1\\1\end{Bmatrix} - \begin{Bmatrix}q_0^{bc}\\-q_L^{bc}\end{Bmatrix} \qquad (37)$$

A direct comparison of the last two sets of elemental matrices illustrates that the so-called modified Picard method is a subset of the more general Newton-Galerkin method and is, therefore, a modified Newton

$$[J_e] = \frac{1}{\Delta t}\left(\frac{L_e}{2}\right)\begin{bmatrix} \partial\theta_1/\partial\psi_1 & 0 \\ 0 & \partial\theta_2/\partial\psi_2 \end{bmatrix} + \frac{1}{L_e}\,\overline{K}\begin{bmatrix} 1 & -1 \\ -1 & 1 \end{bmatrix} \qquad (38)$$

method. The less complete Jacobian explains the slower rate of convergence of the modified Picard method.

Table 1. Brooks-Corey parameters for Yucca Mountain test cases

Soil No.	Thickness (cm)	θ_s	θ_r	b	K_s (cm/s)
1	150	0.27	0.031	5.5	4.9×10^{-3}
2	100	0.25	0.039	6.5	1.0×10^{-3}
3	1,000	0.32	0.082	5.5	2.3×10^{-4}
4	100	0.14	0.086	3.1	4.4×10^{-8}

Table 2. van Genuchten parameters for INEL test cases

Soil No.	Thickness (cm)	θ_s	θ_r	α (1/cm)	n	K_s (cm/s)
1	500	0.503	0.133	0.0169	1.630	2.083×10^{-3}
2	1,500	0.230	0.015	0.0384	1.474	2.778×10^{-4}
3	300	0.145	0.001	0.1000	3.000	3.390×10^{-2}
4	200	0.510	0.120	0.0250	1.590	5.278×10^{-4}
5	500	0.230	0.015	0.0384	1.630	2.778×10^{-4}

Table 3. van Genuchten parameters for Hanford test cases

Soil No.	Thickness (cm)	θ_s	θ_r	α (1/cm)	n	K_s (cm/s)
1	1,200	0.288	0.030	0.1008	2.9224	6.25×10^{-4}
2	800	0.627	0.106	0.0909	3.1071	3.01×10^{-4}
3	600	0.456	0.047	0.0666	2.6751	9.38×10^{-4}
4	1,400	0.451	0.023	0.0116	1.3945	2.31×10^{-5}
5	2,300	0.288	0.030	0.1008	2.9224	6.25×10^{-4}

Table 4. Initial and boundary conditions and simulation times for three case studies: Yucca Mountain (Case 1), Hanford Reservation (Case 2), and INEL site (Case 3)

Case	Initial Pressure (cm)	Upper Boundary	Lower Boundary	Simulation Time
1.1	-10^4	0 cm	0 cm	2 days
1.2	-3.0×10^4	5×10^2 cm	0 cm	1.5 days
1.3	-10^4	1.0×10^{-3} cm/s	$\partial\psi / \partial z = 0$	2 days
1.4	-3.0×10^4	1.0×10^{-3} cm/s	$\partial\psi / \partial z = 0$	2 days
2.1	-5×10^3	0 cm	0 cm	50 yrs
2.2	-10^4	10^2 cm	0 cm	50 yrs
2.3	-5×10^3	10^{-7} cm/s	$\partial\psi / \partial z = 0$	50 yrs
2.4	-10^4	10^{-7} cm/s	$\partial\psi / \partial z = 0$	50 yrs
3.1	-10^4	0 cm	0 cm	11 yrs
3.2	-3×10^4	5×10^2 cm	0 cm	15 yrs
3.3	-10^4	10^{-6} cm/s	$\partial\psi / \partial z = 0$	11 yrs
3.4	-3×10^4	10^{-6} cm/s	$\partial\psi / \partial z = 0$	15 yrs

Table 5. Comparison of CPU times and CPU ratios for untransformed and transformed numerical algorithms

Case	CPU Time (min)/CPU Ratio				
	Modified Picard	Newton-Galerkin	Natural Log	Inverse Hyperbolic Sine	Algebraic
1.1	2.18/3.6	0.60/1.0	0.65/1.1	0.67/1.1	0.75/1.3
1.2	2.65/2.5	1.05/1.0	1.10/1.1	1.83/1.7	1.20/1.1
1.3	1.85/3.1	0.60/1.0	0.63/1.1	0.65/1.1	0.72/1.2
1.4	1.88/3.0	0.62/1.0	0.67/1.1	0.65/1.1	0.73/1.2
2.1	34.33/2.0	17.10/1.0	20.20/1.2	20.43/1.2	24.48/1.4
2.2	30.75/1.9	16.32/1.0	19.60/1.2	19.38/1.2	29.50/1.8
2.3	34.50/3.5	12.47/1.3	NC	NC	9.83/1.0
2.4	23.00/1.3	17.83/1.0	NC	NC	22.62/1.3
3.1	123.93/1.8	69.20/1.0	100.05/1.4	93.30/1.3	96.61/1.4
3.2	120.33/4.9	112.82/1.0	63.88/3.7	126.93/1.4	NC
3.3	118.77/1.7	69.73/1.0	164.25/2.4	162.16/2.3	82.22/1.2
3.4	156.15/2.9	135.15/1.0	298.13/1.1	303.91/2.1	102.72/12.3

NC = non-convergent run

Table 6. Comparison of grid hydraulic Courant numbers used in tests cases

Case	Maximum Co_{hg} Used to Control Time Step Size				
	Modified Picard	Newton-Galerkin	Natural Log	Inverse Hyperbolic Sine	Algebraic
1.1	10	10	10	10	10
1.2	10	10	10	10	10
1.3	10	10	10	10	10
1.4	10	10	10	10	10
2.1	5	5	5	5	5
2.2	5	5	5	5	5
2.3	5	5	<1 (NC)	<1 (NC)	5
2.4	5	5	<1 (NC)	<1 (NC)	5
3.1	5	5	5	5	5
3.2	5	5	5	5	NC
3.3	5	5	1	1	5
3.4	5	5	1	1	5

NC = non-convergent run

Table 7. Comparison of global mass balance errors for untransformed and transformed numerical algorithms

Case	Global Mass Balance Error				
	Modified Picard	Newton-Galerkin	Natural Log	Inverse Hyperbolic Sine	Algebraic
1.1	3.1×10^{-10}	2.4×10^{-14}	1.3×10^{-10}	1.4×10^{-10}	2.8×10^{-11}
1.2	3.6×10^{-10}	3.6×10^{-14}	2.6×10^{-11}	2.0×10^{-10}	2.7×10^{-10}
1.3	1.0×10^{-8}	1.0×10^{-8}	1.0×10^{-8}	1.0×10^{-8}	1.0×10^{-8}
1.4	3.9×10^{-10}	3.8×10^{-10}	3.8×10^{-10}	3.8×10^{-10}	3.1×10^{-10}
2.1	1.5×10^{-8}	1.4×10^{-14}	3.0×10^{-13}	2.7×10^{-16}	8.9×10^{-12}
2.2	1.0×10^{-8}	2.3×10^{-14}	2.6×10^{-12}	6.4×10^{-15}	8.2×10^{-12}
2.3	1.3×10^{-11}	1.0×10^{-12}	NC	NC	2.3×10^{-13}
2.4	4.5×10^{-12}	3.0×10^{-13}	NC	NC	3.4×10^{-14}
3.1	7.2×10^{-9}	4.3×10^{-13}	9.0×10^{-11}	1.8×10^{-12}	3.2×10^{-10}
3.2	1.2×10^{-8}	3.4×10^{-13}	2.4×10^{-11}	1.0×10^{-12}	NC
3.3	3.3×10^{-7}	2.9×10^{-7}	2.7×10^{-7}	2.9×10^{-7}	2.5×10^{-7}
3.4	8.3×10^{-7}	8.0×10^{-8}	7.9×10^{-8}	8.0×10^{-8}	3.8×10^{-8}

NC = non-convergent run

LIST OF FIGURES

Fig 1

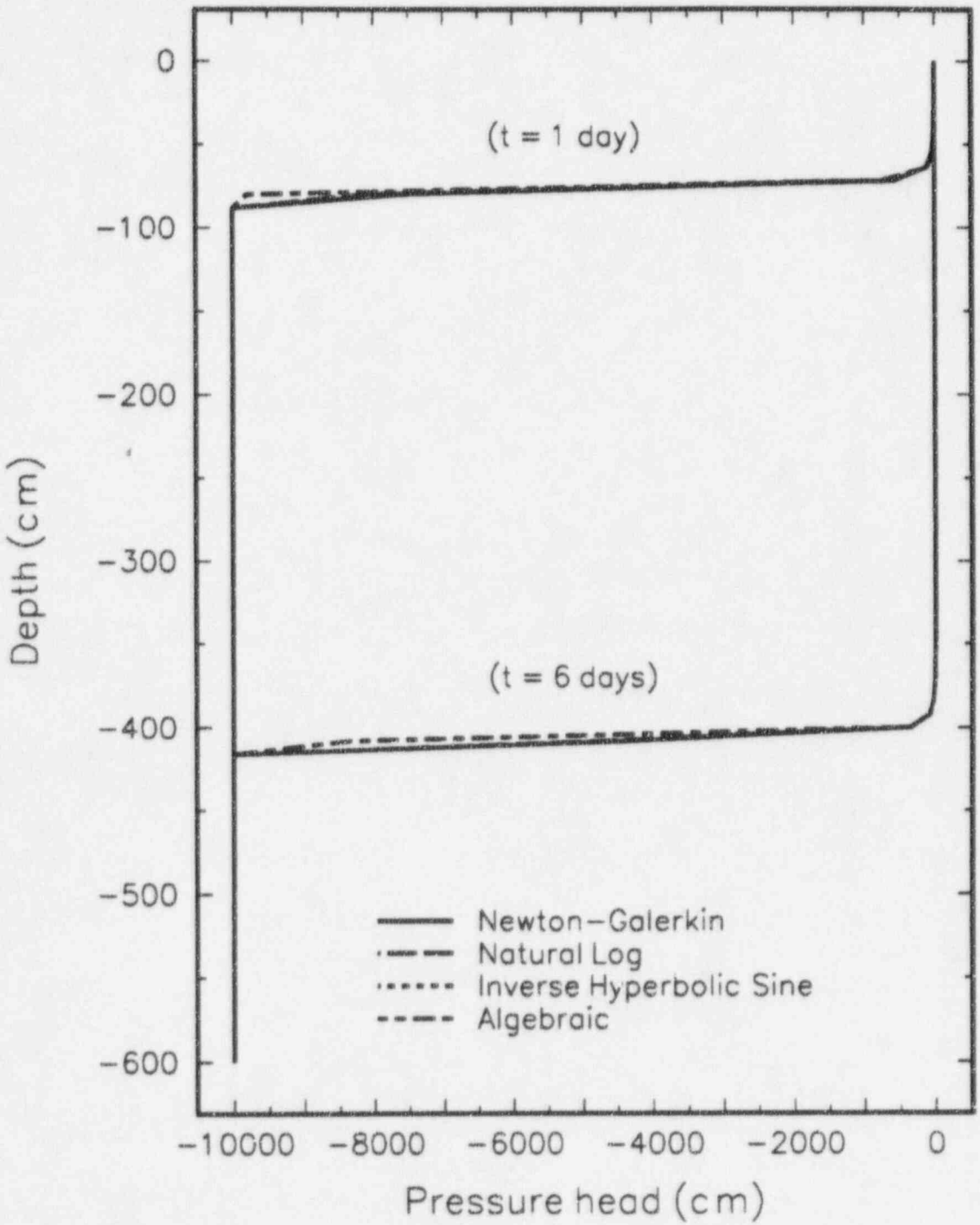
0
-100
-200
-300
-400
-500
-600
Depth (cm)
(t = 1 day)
(t = 6 days)
Newton-Galerkin
Natural Log
Inverse Hyperbolic Sine
Algebraic
-10000
-8000
-6000
-4000
-2000
0
Pressure head (cm)

Fig 2

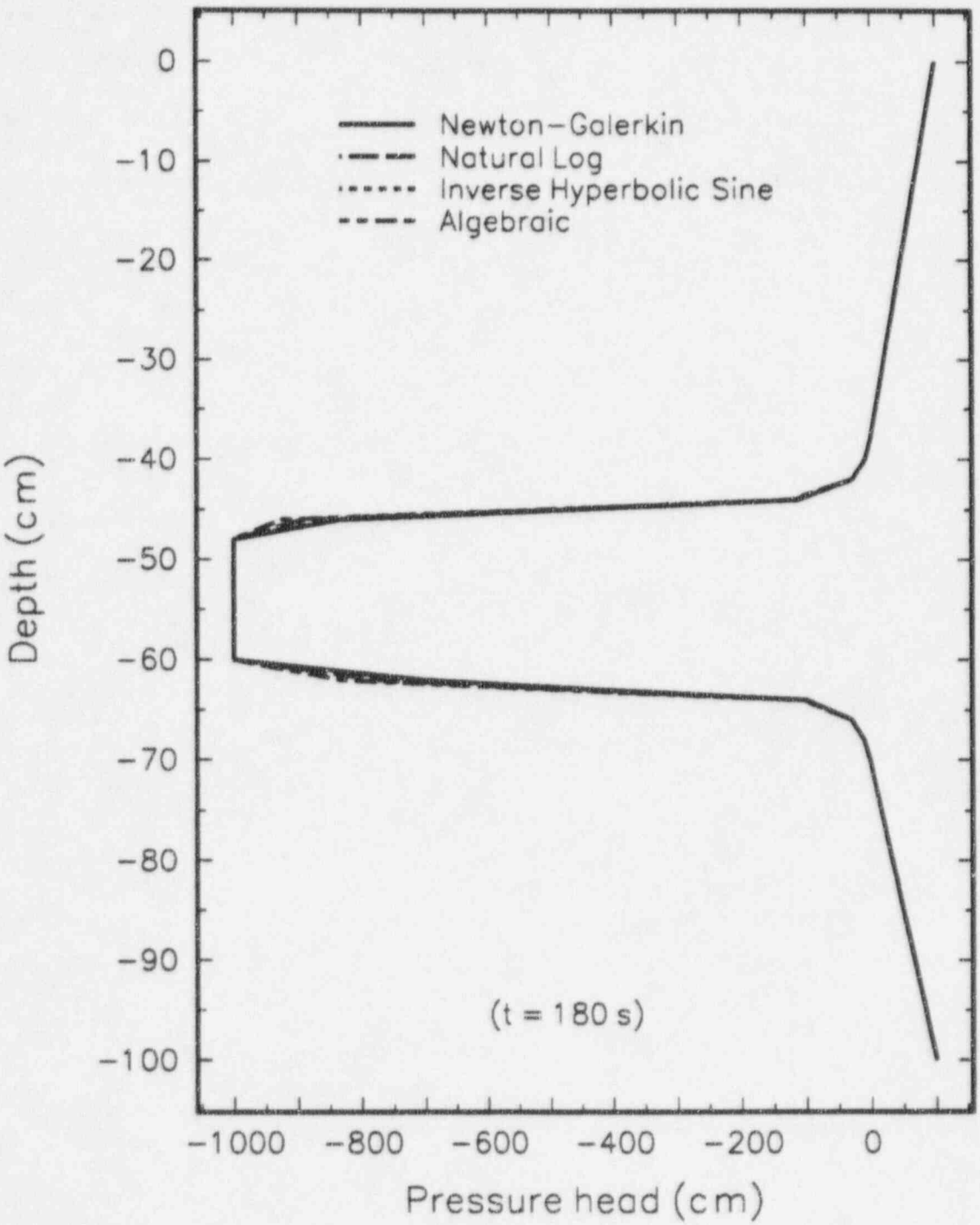
Newton–Galerkin
Natural Log
Inverse Hyperbolic Sine
Algebraic
(t = 180 s)
Depth (cm)
0
-10
-20
-30
-40
-50
-60
-70
-80
-90
-100
-1000
-800
-600
-400
-200
0
Pressure head (cm)

Fig 3a (Verification Test 1)

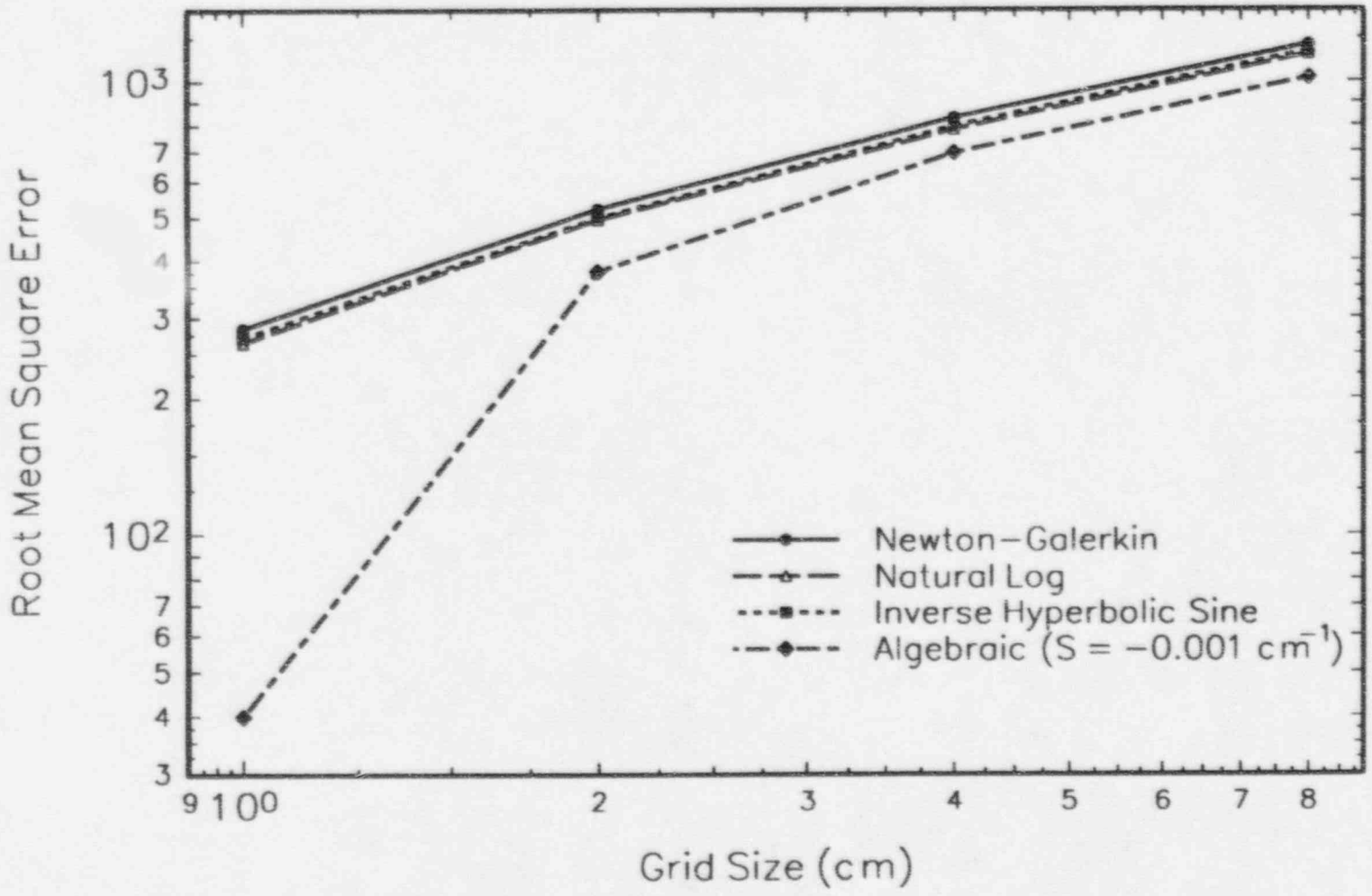

Fig 3b (Verification Test 2)

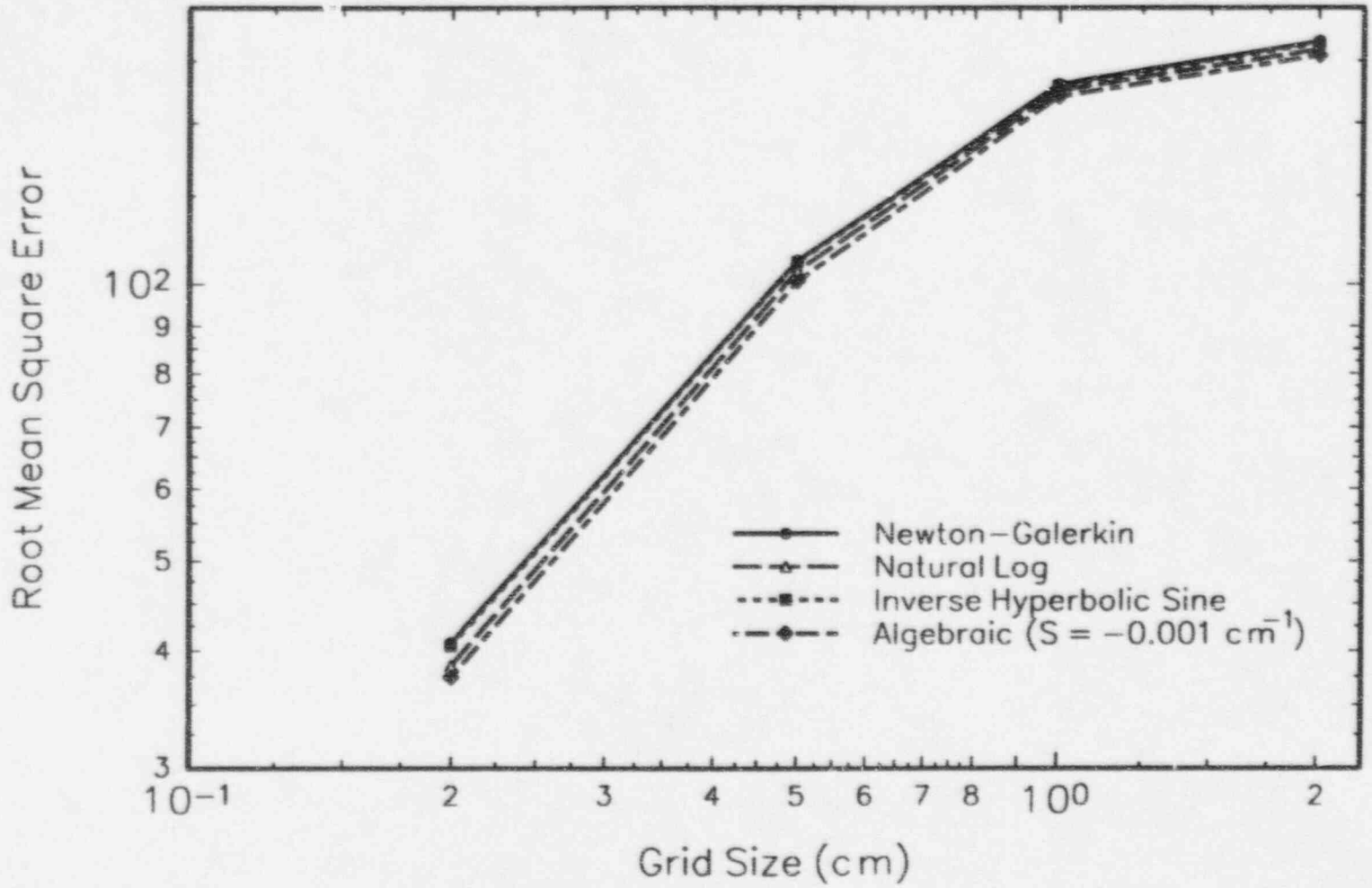

Fig 4a

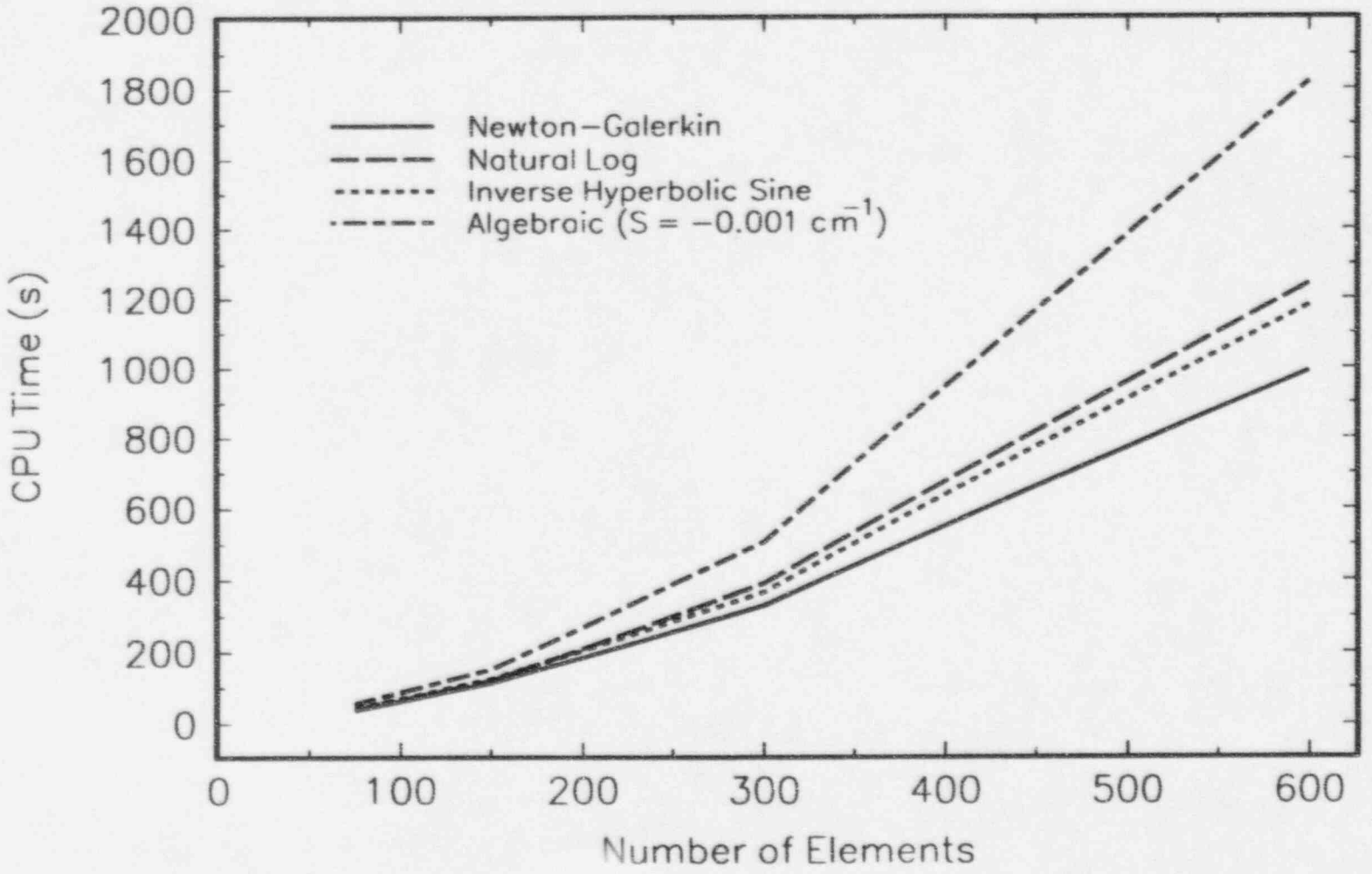
2000
1800
1600
1400
1200
1000
800
600
400
200
0
CPU Time (s)
0
100
200
300
400
500
600
Number of Elements
Newton–Galerkin
Natural Log
Inverse Hyperbolic Sine
Algebraic (S = −0.001 cm⁻¹)

Fig 4b

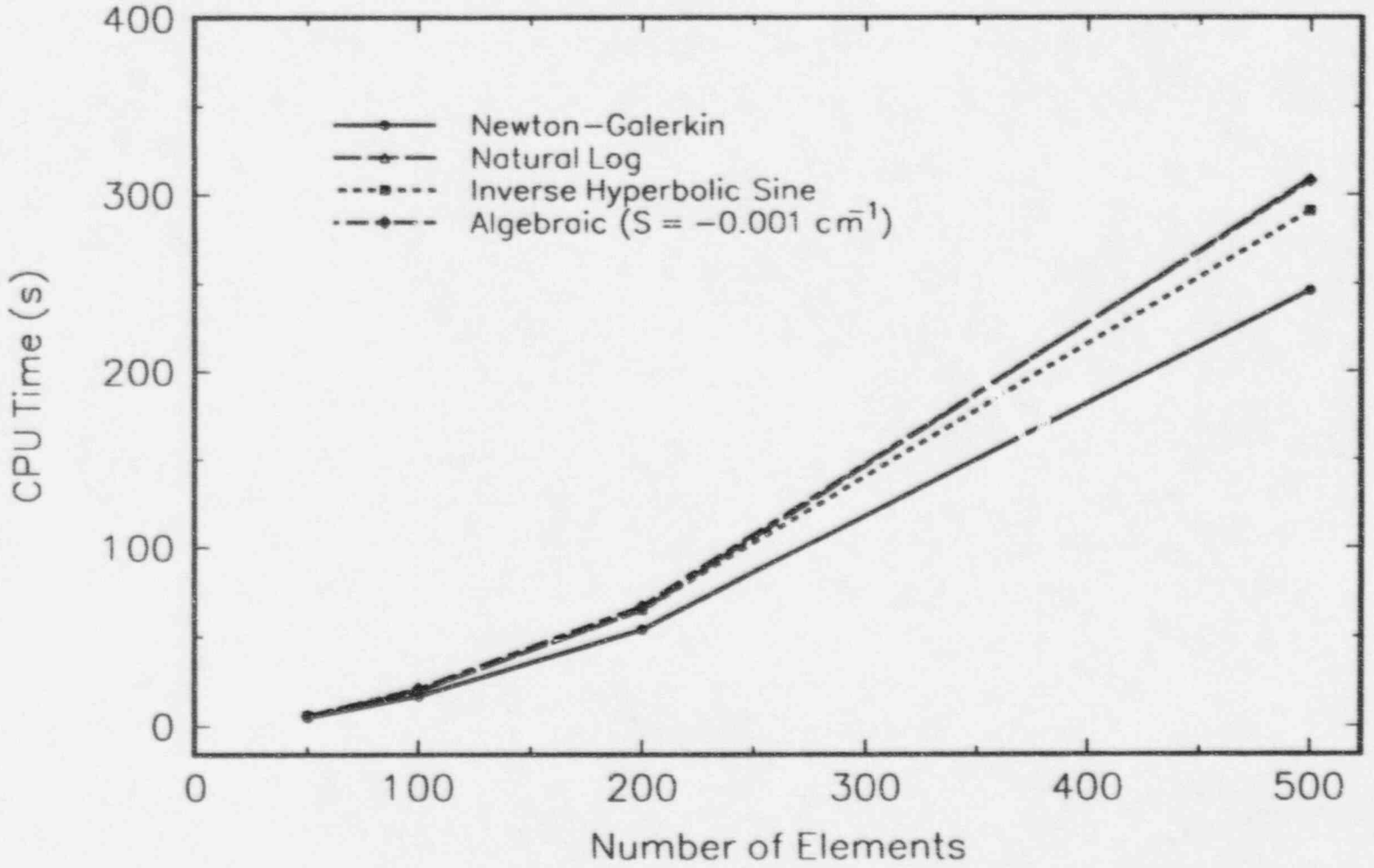
400
300
200
100
0
CPU Time (s)
0
100
200
300
400
500
Number of Elements
Newton–Galerkin
Natural Log
Inverse Hyperbolic Sine
Algebraic (S = −0.001 cm⁻¹)

Figure 5a. Pressure head profiles for Yucca Mountain data set

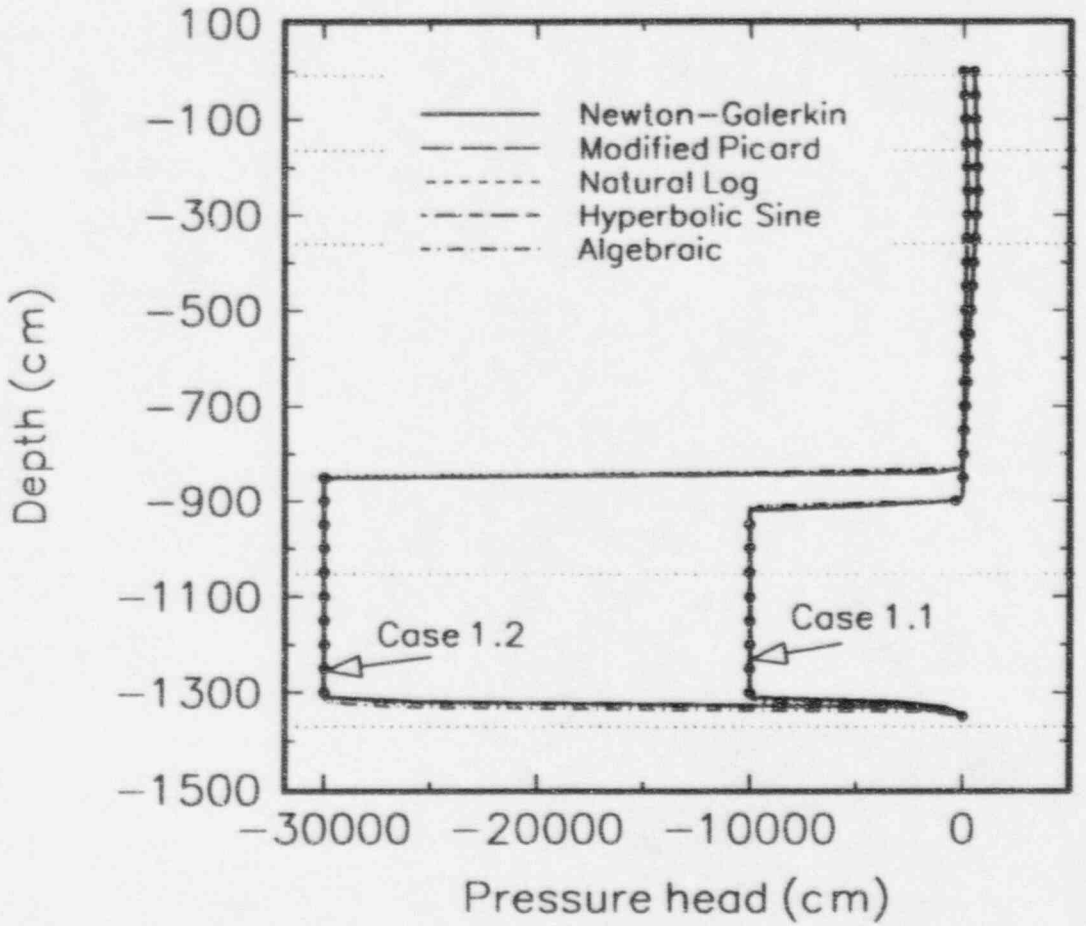

Figure 5b. Pressure head profiles for Yucca Mountain data set

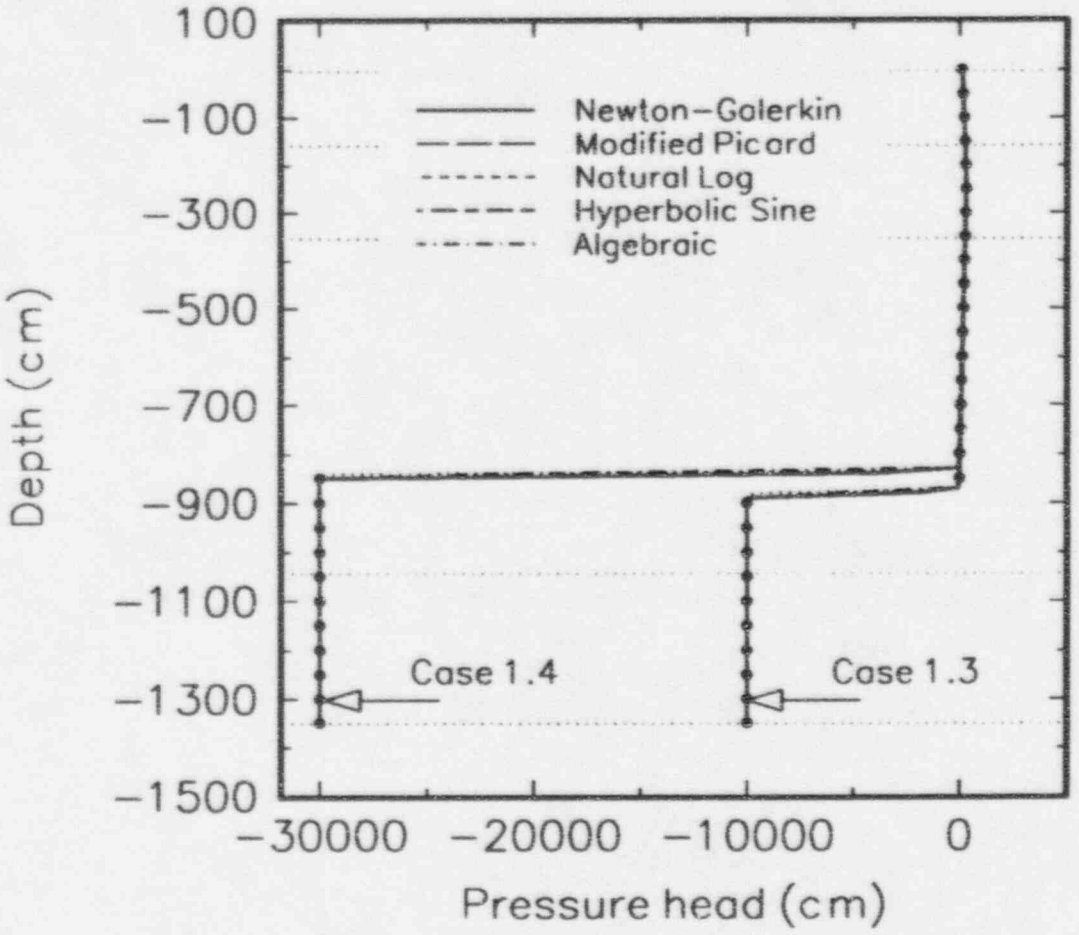

Figure 6a. Pressure profiles for INEL Site

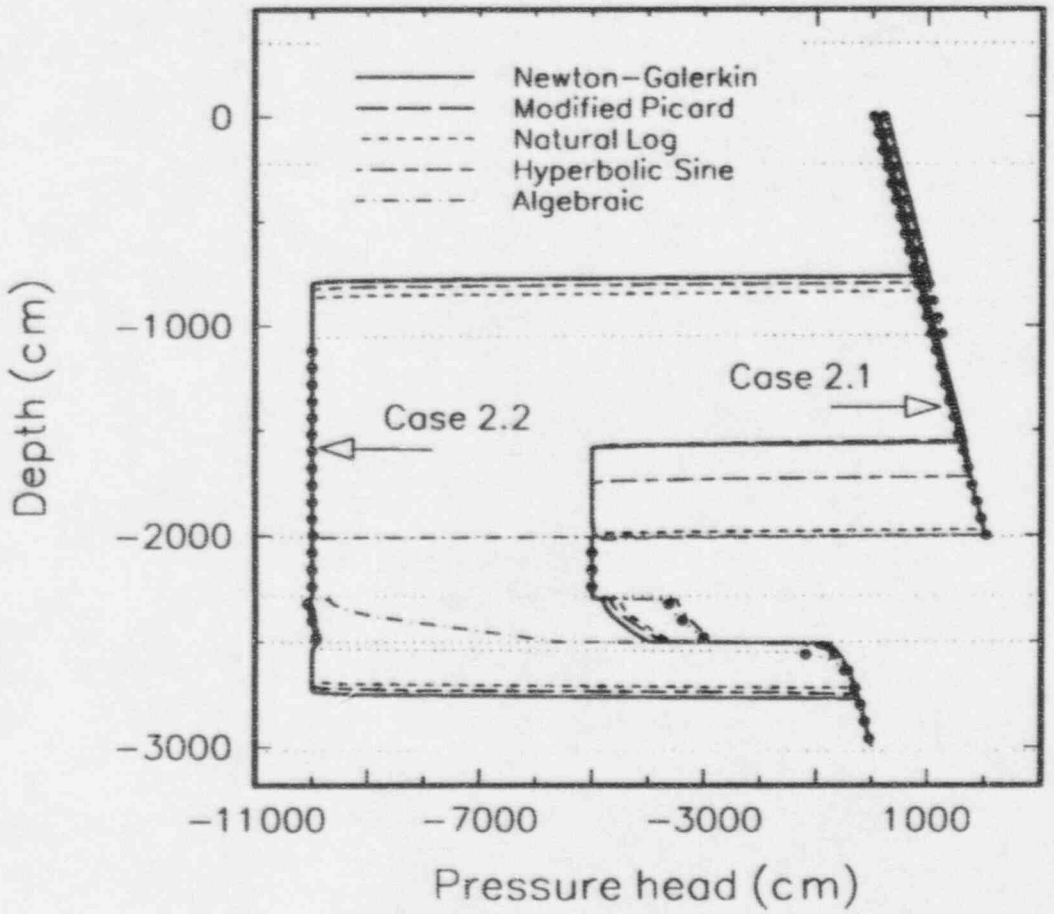

Figure 6b. Pressure profiles for INEL Site

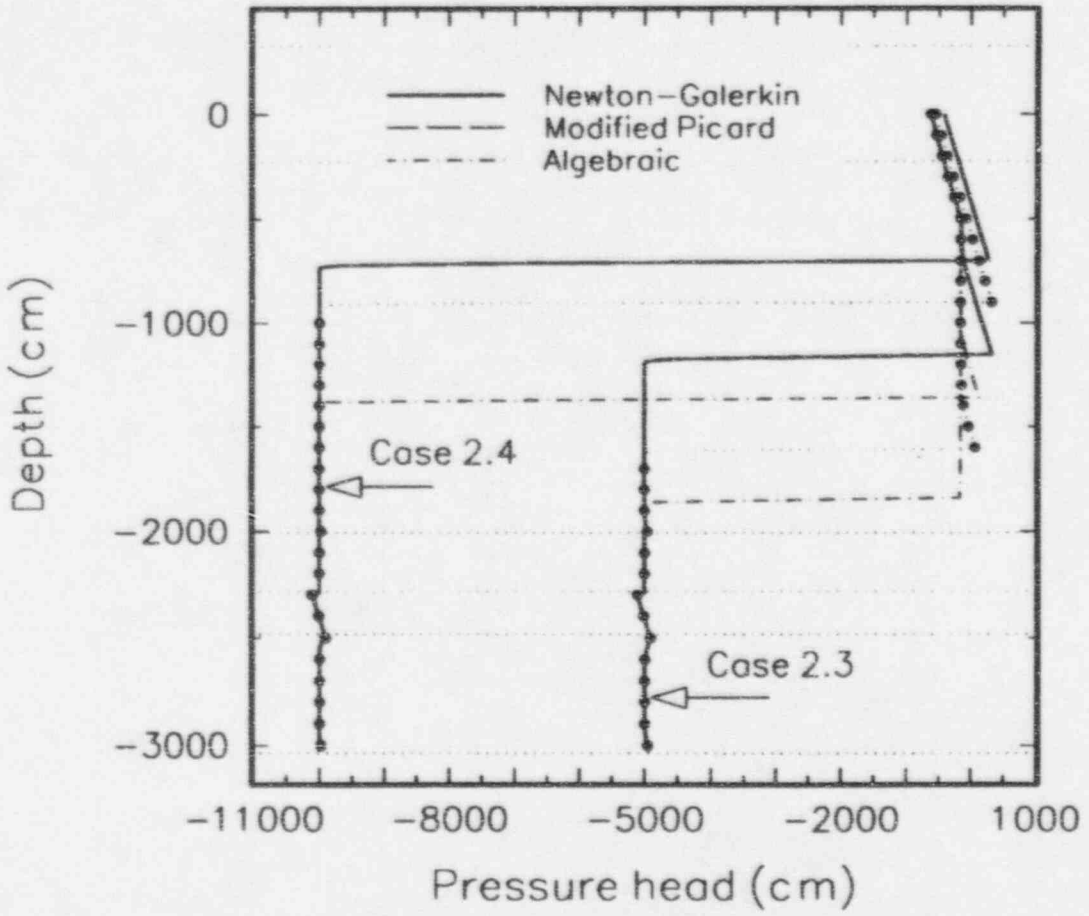

Figure 7a. Pressure head profiles for Hanford Site

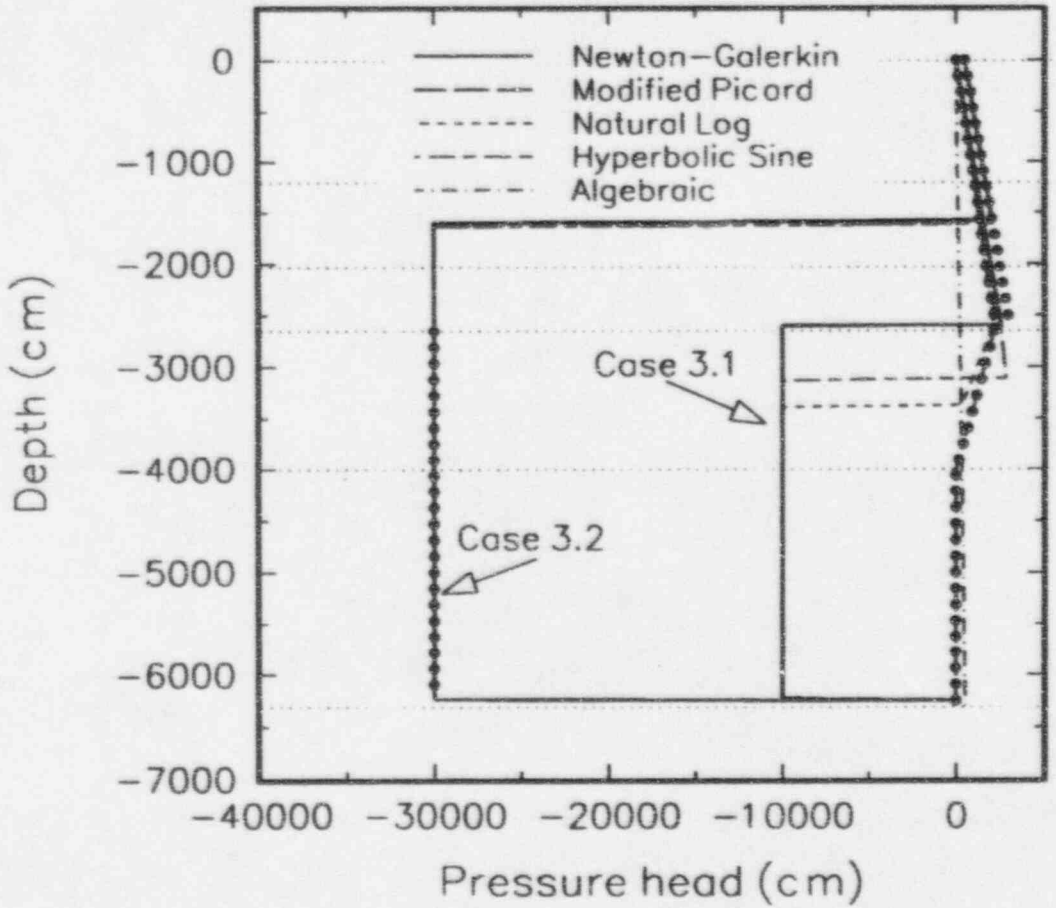

Figure 7b. Pressure head profiles for Hanford Site